PERGAMON

International Journal of Heat and Mass Transfer 45 (2002) 519–531

International Journal of HEAT and MASS TRANSFER

www.elsevier.com/locate/ijhmt

Exploring injected droplet size effects on steady liquid penetration in a Diesel spray with a two-fluid model

V.A. Iyer [a], J. Abraham [a,*], V. Magi [b]

[a] *School of Mechanical Engineering, Purdue University, West Lafayette, IN 47907, USA*
[b] *University of Basilicata, Basilicata, Italy*

Received 27 December 2000; received in revised form 1 May 2001

Abstract

An approach to include droplet size effects in a two-fluid model for Diesel sprays when the locally-homogeneous flow (LHF) assumption is employed is developed. The model is then employed to study the effect of droplet sizes on the steady liquid penetration in vaporizing Diesel sprays when several injection and chamber parameters are changed. These parameters include the orifice diameter, injection pressure, ambient temperature and the ambient density. The computed steady liquid penetration is compared with constant volume measurements made under Diesel conditions at the Sandia National Laboratories. It appears that under typical Diesel conditions, the steady liquid penetration is controlled by entrainment and mixing alone. However, at lower ambient densities, droplet sizes may also be important.

1. Introduction

Multidimensional computations of Diesel sprays have traditionally employed a Lagrangian framework for the liquid in which droplets are treated as discrete particles that are tracked in space and time [1–3]. The gas-phase is treated in an Eulerian manner. Sub-models for atomization, drop dispersion, drop collisions and coalescence, secondary drop break-up and vaporization are employed [1,4–6]. The most important limitation of this procedure is that it is not possible to go to high numerical grid resolution that is required for adequate representation of Diesel sprays [7–10]. This is because the volume fraction of the computational cell occupied by the liquid becomes relatively large (typically greater than 10%) at high resolutions and this leads to numerical instabilities. In any case, the formulation of the equations is only valid for dilute sprays. Because of this limitation, it is difficult to achieve grid-independence with Lagrangian models. Indeed, it has been shown that the collisions and coalescence sub-models do not give converged results [9]. Furthermore, it has been shown that the results are unreasonably sensitive to the selected ambient turbulence parameters at insufficient resolution [7,8]. The degree of sensitivity would depend on the details of the atomization model. Comparisons of the liquid penetration computed with the Lagrangian model with measurements were recently presented in literature [10]. However, the coarse resolution makes the evaluation difficult as there is large numerical diffusion that artificially increases the mixing in the spray. In the present work, a two-fluid model that solves Eulerian field equations for both the gas and the liquid phases are employed to compute liquid-phase penetration. This approach allows us to utilize adequate grid resolution to obtain grid-independent results. The computed liquid-phase penetrations are compared with constant volume measurements in Diesel sprays [11]. The objective of the present study is to assess droplet size effects on the steady liquid penetration in vaporizing Diesel sprays.

2. The contribution of this work

A two-fluid model for Diesel sprays with the locally-homogeneous flow (LHF) assumption that we have discussed in a prior work [12] is modified to include the

* Corresponding author. Tel.: +1-765-494-1505; fax: +1-765-494-0530.
E-mail address: jabraham@ecn.purdue.edu (J. Abraham).

0017-9310/02/$ - see front matter
PII: S0017-9310(01)00168-5

Nomenclature

c_a	specific heat of ambient at constant volume (J/kg K)
c_l	specific heat of liquid at constant volume (J/kg K)
c_p	specific heat of mixture at constant pressure (J/kg K)
c_v	specific heat of vapor at constant volume (J/kg K)
c_{pg}	specific heat of the gas at constant pressure (J/kg K)
D	Sauter mean drop diameter (m)
D_0	injected drop diameter (m)
D_{chamb}	chamber-averaged Sauter mean drop diameter (m)
E	total energy per unit mass (J/kg)
K	vaporization rate constant (1/s)
L	latent heat of vaporization (J/kg)
L_s	surface area concentration per unit mass, (m^2/kg)
M_a	molecular weight of ambient (kg/kmol)
M_v	molecular weight of vapor (kg/kmol)
P	pressure (N/m^2)
$P_{v,s}$	vapor pressure near the droplet surface (N/m^2)
R_u	universal gas constant (J/kmol K)
T	mixture temperature (K)
t	time (s)
T_l	injected liquid temperature (K)
T_s	droplet surface temperature (K)
u_a	specific internal energy of ambient (J/kg)
u_l	specific internal energy of liquid (J/kg)
u_v	specific internal energy of vapor (J/kg)
$\bar{V}$	mixture velocity (m/s)
Y_a	mass fraction of ambient
Y_l	mass fraction of liquid
Y_v	mass fraction of vapor in the two-phase mixture
$Y_{v,g}$	mass fraction of the vapor in the gas phase
$Y_{v,s}$	mass fraction of the vapor in the gas near the droplet surface
Z	mixture fraction
λ_g	thermal conductivity of the gas (W/m K)
ν_t	turbulent diffusivity (m^2/s)
ρ_l	liquid density (kg/m^3)
ρ_m	mixture density (kg/m^3)
$\bar{\tau}_t$	turbulent shear stress tensor (N/m^2)

Subscripts

a	ambient
g	gas
l	liquid
m	mixture
t	turbulent
v	vapor

effect of droplet sizes on liquid vaporization. Transport equations for the liquid surface area concentration and the D^2-law are employed to include the size effects. The model is employed to compare computed and measured steady liquid penetrations in Diesel sprays under a variety of injection and ambient conditions. This is the first time that the droplet size effects have been included in a two-fluid Eulerian-liquid–Eulerian-gas model to study droplet size effects in Diesel sprays. In Section 3, the two-fluid model including the equations that represent the droplet size effects is presented. The numerical procedure and computational conditions are then described in Section 5. In Section 6, discussions and results are presented to illustrate the behavior in a typical Diesel spray and then for changes in steady liquid penetration as the orifice diameter, injection pressure, ambient temperature and ambient density are varied. The paper concludes in Section 7.

3. The two-fluid model

The two-fluid field equations are obtained by suitable averaging of the instantaneous equations of continuity, momentum and energy for each phase [13,14]. The field equations contain source terms accounting for the mass, momentum and energy interactions between the phases [15,16]. The development of the constitutive relations for the two-fluid interactions is a topic of active research and modeling of complex phenomenon such as droplet collisions and coalescence within the context of two-fluid modeling is still in its infancy. The present work employs an LHF assumption [17] in which the gas and the liquid velocities are assumed to be the same and the turbulence in the liquid phase is assumed to follow the gas-phase turbulence. The LHF assumption may be reasonable for Diesel sprays as the large injection velocities atomize the spray into very small droplets whose Stokes numbers are very small. Therefore, the transfer of momentum between the phases is very rapid and the velocities of the two-phases are expected to be identical within a few diameters downstream of the orifice. Separated flow effects may be important near the nozzle exit because of the presence of larger drops. But such large drops may break up into smaller drops within a few effective diameters from the orifice. The LHF assumption reduces the complexity of the problem as only one momentum equation needs to be solved as in a single-phase gas jet computation. The momentum interaction terms vanish. The k–ϵ model [18] has been employed to represent

turbulence. The governing equations of the LHF model are summarized below.

The equation for the overall conservation of mass in the two-fluid mixture is obtained by summing the continuity equations for the two phases [13].

$$\partial\rho_m/\partial t + \nabla\cdot(\rho_m\bar{V}) = 0, \tag{1}$$

where ρ_m is the mixture density and $\bar{V}$ is the ensemble-averaged velocity that is assumed same for the two phases. Assuming incompressible liquid and ideal gas equation of state for the fuel vapor and the ambient air, the mixture density is expressed as

$$1/\rho_m = Y_l/\rho_l + (TR_u/P)(Y_v/M_v + Y_a/M_a), \tag{2}$$

where Y_l, Y_v and Y_a are the mass fractions of the liquid, vapor and ambient air, respectively, T is the mixture temperature and P is the pressure. R_u, M_v and M_a are the universal gas constant and the molecular weights of the vapor and the air, respectively.

The transport equation for the ensemble-averaged mixture momentum equation is obtained by summing the momentum equations for each phase that leads to the cancellation of the interaction terms [13].

$$\partial\rho_m\bar{V}/\partial t + \nabla\cdot(\rho_m\bar{V}\bar{V}) = -\nabla P + \nabla\cdot\bar{\tau}_t \tag{3}$$

where $\bar{\tau}_t$ is the turbulent shear stress tensor that is obtained by solving the standard k–ϵ transport equations [18].

The transport equation for the ensemble-averaged total energy is given by

$$\partial\rho_m E/\partial t + \nabla\cdot(\rho_m\bar{V}E) = \nabla\cdot(P\bar{V}) + \nabla\cdot\rho_m c_p v_t\nabla T, \tag{4}$$

where E is the total energy per unit mass and v_t is the turbulent diffusivity. E is the sum of the kinetic and the internal energies of the different species. It is defined as

$$E = \bar{V}\cdot\bar{V}/2 + Y_l u_l + Y_v u_v + Y_a u_a, \tag{5}$$

where u_l, u_v, u_a are the specific internal energies of the liquid, vapor and the ambient air, respectively. The reference temperature for the specific internal energies is taken to be equal to the temperature at which the liquid fuel is injected. The specific internal energy of the vapor should include the latent heat of vaporization that is absorbed by the vapor when it is formed from the liquid. We can express the specific internal energies in terms of the latent heat and the specific heat capacities of the species at constant volume.

$$u_l = c_l(T - T_l), \tag{6}$$

$$u_v = c_l(T_s - T_l) + L + c_v(T - T_s), \tag{7}$$

$$u_a = c_a(T - T_l). \tag{8}$$

The specific heat capacities, c_l, c_v, c_a, are in general functions of temperature. The latent heat of vaporization, L, is evaluated at the surface temperature of the droplet, T_s. The surface is assumed to be at the thermodynamic wet-bulb temperature as discussed in Section 4. The mixture temperature, T, is calculated from the total energy by solving Eq. (5), which is nonlinear.

4. The vaporization model

The vaporization model is used to predict the mass fractions of the liquid and the vapor fuel. This is done as follows. An equation for the mixture fraction is formulated to describe the transport of the fuel species. The mixture fraction, Z, is the fraction of the mass of species originating from the injected fuel. In the case of non-combusting vaporizing sprays the mixture fraction is defined as

$$Z = Y_l + Y_v. \tag{9}$$

The transport equation for Z is obtained from the conserved scalar formulation [17,19], Z being the conserved scalar, to be

$$\partial\rho_m Z/\partial t + \nabla\cdot(\rho_m\bar{V}Z) = \nabla\cdot(\rho_m v_t\nabla Z), \tag{10}$$

where v_t is the turbulent diffusivity obtained from the k–ϵ model assuming that the turbulent Schmidt number is unity. The mixture fraction approach was used in an earlier work where vaporization was modeled using a state relationship [12]. The state relationship was obtained assuming local thermodynamic equilibrium between the two-phases at all points in the flow. In this work, however, we do not assume thermodynamic equilibrium between the liquid and the vapor fuel. Instead, the rate of vaporization is obtained from the D^2-law for single droplet vaporization. According to the D^2-law [19]

$$\mathrm{d}D/\mathrm{d}t = -K/2D, \tag{11}$$

where D is the droplet diameter and

$$K = 8\lambda_g\ln(B_T + 1)/\rho_l c_{pg}, \tag{12}$$

where B_T is the thermal transfer number defined as

$$B_T = c_{pg}(T - T_s)/L \tag{13}$$

and λ_g and c_{pg} are the thermal conductivity and the specific heat of the gas phase near the surface of the droplet, respectively, and they are functions of the temperature and are evaluated at the mean of the surface and the mixture temperature. The surface temperature, T_s, is assumed to be equal to the thermodynamic wet bulb temperature at the local mixture temperature, T, and local vapor mass fraction in the gas, $Y_{v,g}$. The vapor mass fraction in the gas is related to the vapor mass fraction in the two-phase mixture by

$$Y_{v,g} = Y_v/(1 - Y_l). \tag{14}$$

The wet-bulb temperature is obtained by equating the thermal and the mass transfer numbers [20].

$$c_{pg}(T - T_s)/L = (Y_{v,s} - Y_{v,g})/(1 - Y_{v,g}). \tag{15}$$

The surface temperature, T_s, and the surface vapor mass fraction, $Y_{v,s}$, are related by the Antoine equation [1]. The Antoine equation expresses the dependence of the surface vapor pressure on the surface temperature and is given by

$$\log_{10}(P_{v,s}) = A - B/(T_s + C), \tag{16}$$

where the constants A, B and C are empirical constants that depend on the fuel. The surface vapor pressure, $P_{v,s}$, is the product of the local pressure, P and the surface vapor mole fraction in the gas, $X_{v,s}$.

$$P_{v,s} = PX_{v,s}. \tag{17}$$

The surface mole fraction, $X_{v,s}$, can be expressed in terms of the surface mass fraction, $Y_{v,s}$, as

$$X_{v,s} = Y_{v,s}/M_v/\{Y_{v,s}/M_v + (1 - Y_{v,s})/M_a\}. \tag{18}$$

The surface temperature and the surface vapor mass fractions are obtained by the simultaneous solution of Eqs. (15) and (16) using the relations given by Eqs. (14), (17) and (18). The D^2-law as stated by Eq. (11) is assumed to hold locally in the flow. The mass rate of vaporization is obtained from the D^2-law by expressing the liquid mass fraction in terms of the droplet diameter as

$$Y_l = (\pi D^3/6)(\rho_l/\rho_m)(N/V), \tag{19}$$

where N/V is the local number density of the droplets. Differentiating the above equation with respect to time, the number density being constant during the process of vaporization, the mass rate of vaporization is given as

$$\mathrm{d}(\rho_m Y_l)/\mathrm{d}t = -1.5K(\rho_m Y_l)/D^2. \tag{20}$$

The above expression is used as a source term in the transport equation for the liquid mass fraction as shown below

$$\partial(\rho_m Y_l)/\partial t + \nabla\cdot(\rho_m Y_l \bar{V}) = \nabla\cdot(\rho_m \nu_t \nabla Y_l) - 1.5K(\rho_m Y_l)/D^2. \tag{21}$$

The vapor mass fraction, Y_v, is obtained from Eqs. (9) and (10). The mean diameter, D, is not a constant in the flow-field. This is determined as follows. A transport equation for the surface area concentration per unit mass of the mixture, L_s, is written [13] with the vaporization source term obtained in a manner similar to that for the liquid mass fraction.

$$\partial(\rho_m L_s)/\partial t + \nabla\cdot(\rho_m L_s \bar{V}) = \nabla\cdot(\rho_m \nu_t \nabla L_s) - K(\rho_m L_s)/D^2. \tag{22}$$

Eqs. (21) and (22) are solved simultaneously to compute the liquid mass fraction and the surface area concentration. The surface area concentration can be expressed in terms of the local mean diameter, D, of the droplets as

$$L_s = (\pi D^2/\rho_m)(N/V). \tag{23}$$

The local mean diameter, D, of droplets is then obtained by dividing Eq. (19) by Eq. (23), which gives

$$D = (6Y_l)/(\rho_l L_s). \tag{24}$$

We need to specify the size of the droplets at the injector in the model. In the literature, expressions have been proposed for predicting the Sauter mean diameter of droplets that result from atomization [5]. One such model based on the Taylor instability theory that we have employed extensively [9] relates the droplet diameter to the injection velocity and the ambient density by the following expression:

$$D_0 = C/(\rho_a U_{inj}^2), \tag{25}$$

where ρ_a and U_{inj} are the ambient density and the injection velocity, respectively. The constant C depends on the Taylor number and the nozzle geometry. In our work, we will employ the values of D_0 obtained from the expression above when we use the constant, C, proposed in reference [5,9] as well as modified values obtained by changing C. In general, we will use the symbol d_0 to identify the injected Sauter mean drop diameter.

5. The numerical procedure and the computational conditions

The computational domain is shown in Fig. 1. The domain is an axisymmetric chamber with dimensions chosen such that there is minimal interaction of the spray with the walls of the chamber and corresponds approximately to the size of the experimental chamber described below. Notice that very fine grid resolution is used near the jet centerline. There are 10 cells inside the orifice diameter that was found adequate to obtain grid-independent results for the liquid penetration. In typical Lagrangian calculations, the minimum grid size possible is about twice the orifice diameter [7]. The computations are performed for a range of injection pressures, ambient temperatures and ambient densities. Injection velocities are obtained from the injection pressures using a discharge coefficient of 0.78, the value reported for the injector in the measurements [11]. A top-hat exit velocity profile is assumed. The injection and ambient conditions are stated in Table 1. The fuel properties are those for tetradecane and nitrogen is used as the ambient gas. The injected drop sizes as

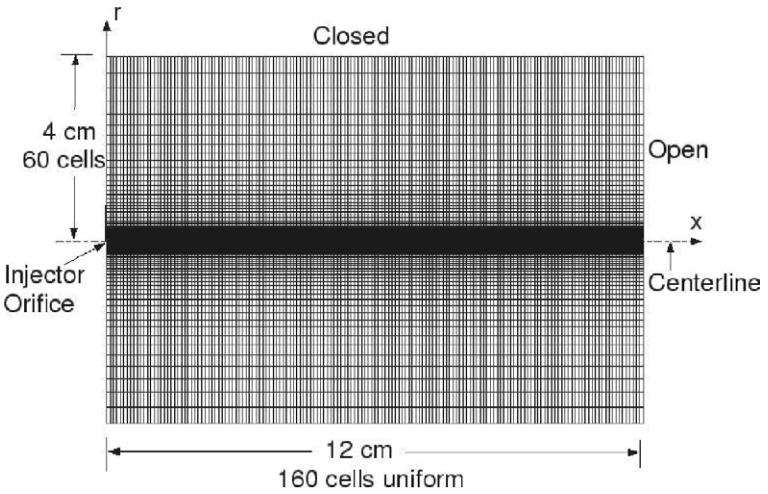

Fig. 1. Computational grid.

Table 1
Injection and ambient conditions

Orifice diameter	100, 246, 350, 500 μm
Injection pressures	65, 90, 120, 136, 170 MPa
Injection velocities	334, 393, 454, 483, 540 m/s
Ambient densities	3.6, 7.3, 14.8, 30.2, 60 kg/m^3
Ambient temperatures	850, 1000 K
Fuel temperature	438 K

predicted by Eq. (25) depend on the injection velocity and the ambient density.

A finite volume numerical method [1] is employed to solve the equations. The computations are transient and each numerical time-level involves solving a pressure equation simultaneously with the momentum equation in an iterative manner similar to the SIMPLE procedure [21]. The iterative procedure at every time level starts by setting up the momentum-pressure dependence. This essentially involves solving the momentum equations in the radial and the axial directions excluding the pressure gradient terms. The pressure equation is then set up by combining the discretized equation for the conservation of mass with the discretized equation for momentum. The pressure equation is an axisymmetric Poisson-type equation that is solved by an Alternate-Direction-Implicit (ADI) scheme. The momentum is then corrected for the pressure gradients. The solution of the pressure and the momentum equations are followed by the solution of the transport equations for mixture fraction, liquid mass fraction, surface area concentration and the energy equations. A first-order upwind scheme is used to approximate the convective fluxes in these transport equations. The mixture and the surface temperatures require solutions of non-linear algebraic equations as discussed in Section 4. A Newton-type iterative scheme is used with the values of the temperatures from the prior iteration taken as the initial guess. The iterations are repeated starting from the momentum equations until convergence of the pressure field is obtained. Typically, convergence is obtained in 3–4 iterations. The turbulence transport equations are solved with the converged flow-field and a new turbulent diffusivity, ν_t, is obtained for the next time level.

The computations are compared with laser diagnostic measurements of non-combusting sprays under Diesel conditions performed by Siebers at Sandia National Laboratories [11]. The measurements were made in a constant volume chamber and the liquid phase penetrations were obtained from Mie-scattered images. The fuel injector was a prototype, electronically controlled common-rail injector designed by Detroit Diesel Corporation. The conditions used in the present work are comparable to the ones employed in the measurements. We have presented prior comparisons of computed results with these measurements by employing the Lagrangian model [10] and the two-fluid model with equilibrium assumptions [12].

6. Results and discussions

Computed results are first shown for a case in which the ambient temperature, T_a, is 1000 K, ambient density, ρ_a, is 30.2 kg/m^3, injection pressure, P_{inj}, is 136 MPa and the orifice diameter, d_{orif}, is 246 μm. These conditions are referred to as the baseline case in subsequent discussions in this section. Fig. 2(a) shows the contour plot of liquid mass fractions in the computational domain for the baseline case at 0.3 and 0.7 ms after the start of injection (ASI). It should be noted that the liquid mass fraction contours in Fig. 2(a) are shown in a small fraction

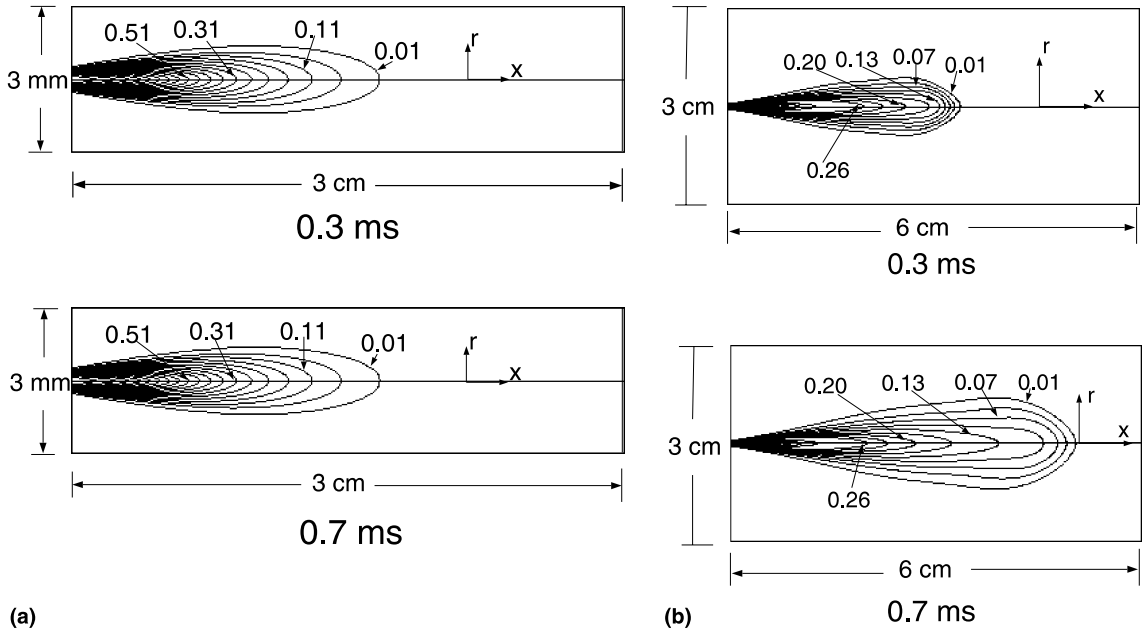

Fig. 2. Liquid and vapor mass fraction contours. $\rho_a = 30.2$ kg/m^3, $T_a = 1000$ K, $P_{inj} = 136$ MPa, $d_{orif} = 246$ μm. Notice that radial and axial scales are different (see text).

(3 mm diameter ×3 cm axial length) of the entire computational domain within which the liquid is contained. The scale in the radial direction is enlarged with respect to the scale in the axial direction so that the radial spread of the mass fraction contours is clearly visible. The figure shows that the liquid mass fraction distribution is identical at 0.3 and 0.7 ms ASI. This implies that the liquid mass fraction distribution reaches a steady state before 0.3 ms for this set of conditions. It is clear from Fig. 2(a) that the radial spread of the liquid is less than 1.5 mm and the axial penetration is less than 2 cm. Fig. 2(b) shows the contour plot of the vapor mass fractions in the computational domain for the baseline case at 0.3 and 0.7 ms ASI. The figure shows that the radial spread of the vapor is about an order of magnitude greater than that of the liquid. The figure also shows that the vapor continues to penetrate axially and spread radially with time as opposed to the liquid that reaches a steady distribution. However there is a steady region even in the vapor distribution upstream of the tip of the jet as seen in Fig. 2(b). This is typical of axisymmetric turbulent jets [22]. We now look at the variation of the mass fractions along the centerline of the jet to get a quantitative description.

Fig. 3 shows the computed liquid and vapor mass fractions along the centerline of the spray at 0.25, 0.5 and 1 ms after the start of injection for the baseline case. The liquid mass fraction curves remain unchanged as a function of time once steady state is achieved, which is in agreement with the observation of Siebers [11]. For this

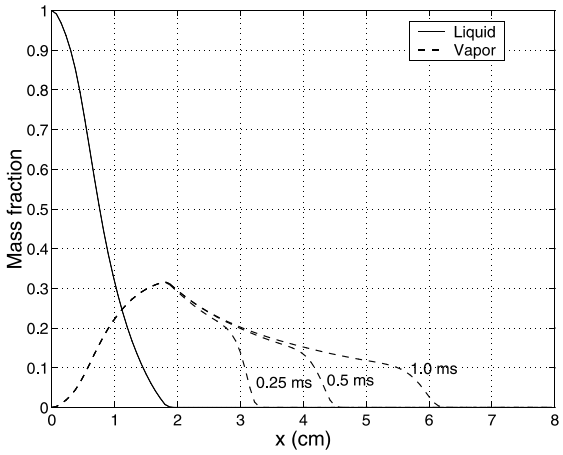

Fig. 3. Liquid and vapor mass fractions along centerline of spray. $\rho_a = 30.2$ kg/m^3, $T_a = 1000$ K, $P_{inj} = 136$ MPa, $d_{orif} = 246$ μm.

condition, steady state is achieved in about 0.25 ms after the start of injection. Fig. 3 may be used to illustrate how the liquid penetration is defined in the vaporizing sprays. The penetration is defined as the axial location along the centerline where the liquid mass fraction reaches 1%. This definition is used to compute the steady liquid penetration for all the cases presented in the rest of the paper. Fig. 3 also shows the computed vapor mass fractions along the centerline of the spray at 0.25, 0.5

and 1 ms after the start of injection. The vapor mass fractions increase from zero at the orifice to a peak value of about 0.32 for this case. The peak value occurs approximately at the axial location where the liquid completely vaporizes. The vapor keeps penetrating further with time as opposed to the liquid that reaches a steady penetration.

We now compare the variation of the mass fractions when the ambient density and the ambient temperatures are changed relative to the baseline case. Fig. 4 shows the variation of the liquid and the vapor mass fraction along the centerline of the spray at 0.5 ms after the start of injection for the baseline case, a case where the ambient temperature is changed to 850 K and a case where the ambient density is changed to 14.8 kg/m^3. The liquid mass fractions increase at all axial locations when the ambient temperature is reduced. Overall, the liquid penetration increases by about 25% when the temperature is reduced to 850 K. The decrease in ambient temperature decreases the energy content of the entrained ambient gas and so vaporization rate is reduced. Similar trends are predicted when the ambient density is decreased to 14.8 kg/m^3. The decrease in the ambient density decreases the mass of the ambient gas entrained and so vaporization rate is reduced. The figure shows that the steady liquid penetration increases by about 25% when the density is reduced to 14.8 kg/m^3. A detailed discussion on the variation of liquid penetration with different ambient and injection conditions follows in later sections. The decrease in ambient temperature decreases the peak value of the vapor mass fraction by about 20–25%, but the overall penetration of the vapor fuel remains the same at the same time. This shows that the change in temperature changes the energy content of the ambient but does not affect the mixing characteristics of the jet due to the relatively incompressible nature of the flow-field. However when the ambient density is reduced to 14.8 kg/m^3, both the peak value of the vapor mass fraction and the vapor fuel penetration increases. Thus, decrease in ambient density increases both the liquid and the vapor fuel mass fractions along the centerline. The decrease in ambient density decreases the amount of mixing and entrainment of ambient air and dispersion of the spray so more fuel remains at the centerline and thus both the liquid and the vapor fractions increase proportionately.

6.1. Variation of liquid penetration with injected drop size

In the computations discussed above, the injected drop size is determined from Eq. (25). What would be the effect of changing this drop size? Fig. 5 shows the computed liquid penetration, as defined earlier, as a function of time when the injected drop diameter is changed as indicated on the figure. Here, D_0 refers to the injected drop diameter as predicted by the atomization model, Eq. (25), and d_0 to the actual injected drop diameter. The orifice diameter, injection pressure, ambient temperature and the ambient density are 246 μm, 136 MPa, 1000 K and 30.2 kg/m^3, respectively. The figure shows that the liquid penetration reaches a steady state for the cases with $d_0 = D_0$, $d_0 = 10D_0$ and $d_0 = 50D_0$ within the duration of the computations. Both the steady penetration value and the time required to reach steady state increases with increase in the injected drop size. This is because the larger drops take more time to vaporize according to the D^2-law. For the case where the injected drop diameter is equal to $100D_0$, a steady penetration is not reached within 1.6 ms. The steady penetration increases by only 10% when the injected drop

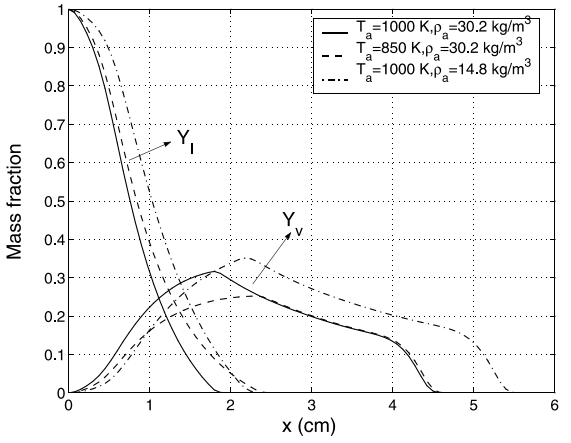

Fig. 4. Liquid and vapor mass fractions along centerline of spray. Effect of decrease in ambient temperature and density. $P_{inj} = 136$ MPa, $d_{orif} = 246$ μm.

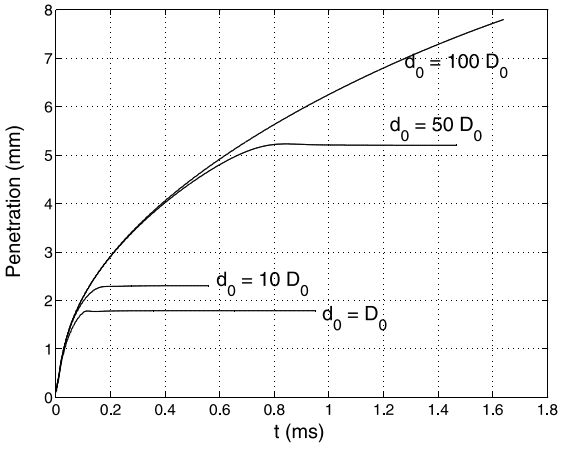

Fig. 5. Liquid penetration versus time for different injected SMD. $\rho_a = 30.2$ kg/m^3, $T_a = 1000$ K, $P_{inj} = 136$ MPa, $d_{orif} = 246$ μm.

diameter is increased to $10D_0$. However, according to the D^2-law, the droplet vaporization rate decreases by a factor of 100 when the drop size increases by a factor of 10. Therefore, if vaporization were controlled by the drop size alone, then the liquid penetration should have increased by two orders of magnitude. However, the predicted increase is only about 10%. This implies that drop size is not the important controlling factor, but the liquid penetration is controlled largely by the amount of air entrained into the spray. However, when the injected drop diameter is increased by a factor of 50, the increase in penetration is about 150% and when the injected drop diameter is $100D_0$, a steady penetration is not reached in 1.6 ms. The results imply that for small injected drop sizes, vaporization is controlled by the mass of air entrained by the spray and the process of vaporization reaches an equilibrium state that is independent of the drop size [12]. For larger injected drop sizes, the drop size becomes an important factor in determining the liquid penetration. The findings of Siebers [11] indicate that the liquid penetration is mixing controlled which, in turn, implies that the drop sizes are relatively small.

6.2. Variation of steady liquid penetration with orifice diameter

We now present comparisons of the computed steady liquid penetration with the measurements made at Sandia National Laboratories [11]. Fig. 6 shows the computed and measured liquid penetrations as a function of the orifice diameter for two cases with ambient densities of 30.2 and 7.2 kg/m^3. The ambient temperature and the injection pressure for both the cases are 1000 K and 136 MPa, respectively. Both the computations and the measurements show that the steady liquid penetration increases almost linearly with increase in orifice diameter. This linear increase in the steady liquid penetration can be explained as follows. The mass of fuel injected in a certain amount of time increases as the square of the orifice diameter. However, according to the theory of entrainment in turbulent jets [11,22], the mass of air entrained in a certain duration of time increases linearly with the orifice diameter. The mass of fuel vaporized is proportional to the mass of air entrained when other factors such as temperature and droplet size are kept constant. Therefore, a balance of the injected and the vaporized mass shows that the mass of fuel vaporized per unit mass of fuel injected should decrease inversely with the orifice diameter. As a result, the liquid penetration increases linearly with orifice diameter. The computations are able to predict this expected trend. The figure also shows that the quantitative agreement is within 5% at the ambient density of 30.2 kg/m^3, but the computations under-predict the measured values by about 30% at the higher ambient density of 7.2 kg/m^3. The explanation of the quantitative disagreement at lower densities will be discussed in a later section when we discuss the trend with ambient density.

6.3. Variation of steady liquid penetration with injection pressure

Fig. 7 shows the computed and measured steady liquid penetrations as a function of the injection pressure for two different ambient densities of 30.2 and 7.2 kg/m^3. The ambient temperature and orifice diameter are 1000 K and 246 μm, respectively. The computations for the ambient density of 30.2 kg/m^3 predict that the steady liquid penetration is approximately independent of the injection pressure. This is consistent with the measured trend. Increasing the injection pressure in-

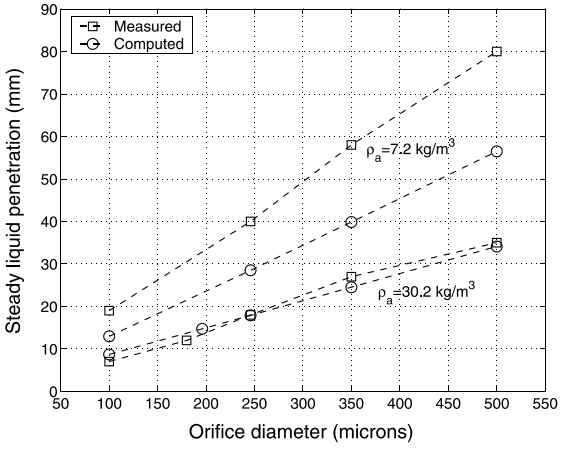

Fig. 6. Steady liquid penetration versus orifice diameter. $T_a = 1000$ K, $P_{inj} = 136$ MPa.

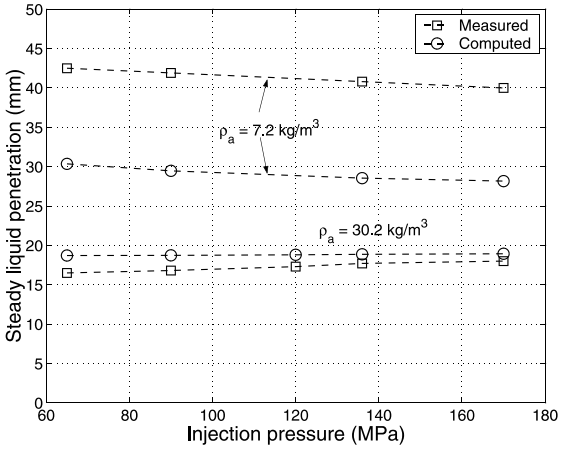

Fig. 7. Steady liquid penetration versus injection pressure. $T_a = 1000$ K, $d_{orif} = 246$ μm.

creases the injection velocity, so more mass of fuel is injected in a given time. However, there is a proportional increase in the mass of air entrained into the jet [22]. Therefore, a balance of the injected mass of fuel and the entrained mass of air predicts the liquid penetration to be independent of the injection pressure. This is based on the assumption that the mass of fuel vaporized is proportional to the mass of air entrained. However, as we increase the injection pressure, the injected drop size decreases according to the atomization model, Eq. (25). We have seen earlier in Fig. 6 that smaller drops tend to vaporize faster and penetrate less. However, for the ambient density of 30.2 kg/m^3, the injected drop sizes are small enough that vaporization appears to be controlled primarily by entrainment of the ambient air. Therefore, the mass of fuel vaporized is indeed proportional to the mass of air entrained and the liquid penetration is insensitive to the injection pressure.

At the lower ambient density of 7.2 kg/m^3, the measurements again show that the liquid penetration is approximately independent of the injection pressure. There is a small decrease of about 5–10% in the liquid penetration in both measurements and computations when the injection pressure is increased from 65 to 170 MPa. This decrease may be due to the decrease in drop sizes. To assess this we performed computations where the injected drop size is kept constant as we vary the injection pressure. Fig. 8 shows the computed steady liquid penetration as a function of the injection pressure for the ambient density of 7.2 kg/m^3 when the injected drop size is fixed for all the cases to that corresponding to the injection pressure of 65 MPa. The figure shows that the steady liquid penetration remains almost constant when the injected drop size is fixed as compared to the earlier case when the injected drop size is varied with injection pressure according to Eq. (25). This implies that the decrease in the steady liquid penetration with increase in the injection pressure as shown in Fig. 7 is due to the decrease in injected drop sizes when the injection pressure is increased. Thus, the computations predict the measured trends with reasonable accuracy. The quantitative agreement between the measurements and the computations is better at the higher ambient density. At the lower ambient density, the computations under-predict the liquid penetration by about 35%. Overall, both the computed and the measured trends show that the liquid penetration is controlled by entrainment of the ambient air and that drop size effects are secondary for the relatively large injection pressures typical of Diesel injectors.

6.4. Variation of steady liquid penetration with ambient temperature

Fig. 9 shows the computed and the measured steady liquid penetrations as a function of the ambient temperature for two different ambient densities of 30.2 and 14.8 kg/m^3. The injection pressure and the orifice diameter are 136 MPa and 246 μm, respectively. Based on the atomization model, the size of the droplets does not change with ambient temperature. The computed trend shows reasonable agreement with the measured trend in that the penetration decreases with increase in ambient temperature. Increase in temperature increase the energy content of the entrained air and so the mass of the injected fuel vaporized increases proportional to the ambient temperature. Thus, the steady liquid penetration shows an inverse dependence on the ambient temperature. As for the earlier cases, the quantitative agreement is within 5% for the ambient density of 30.2 kg/m^3,

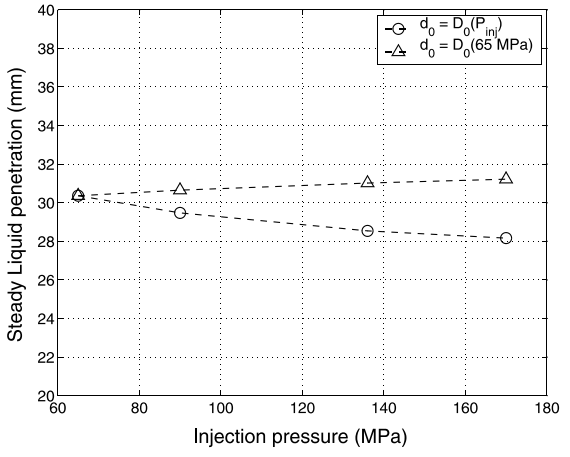

Fig. 8. Steady liquid penetration versus injection pressure. Effect of injected drop size variation. $\rho_a = 7.2$ kg/m^3, $T_a = 1000$ K, $d_{orif} = 246$ μm.

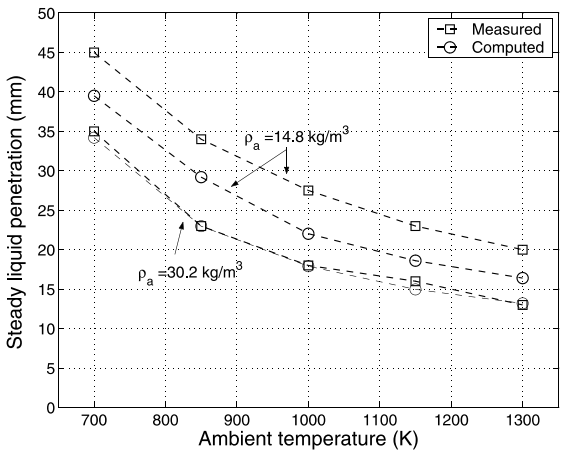

Fig. 9. Steady liquid penetration versus ambient temperature. $\rho_a = 30.2$ kg/m^3, $P_{inj} = 136$ MPa, $d_{orif} = 246$ μm.

whereas for the lower ambient density, the computed penetration under-predicts the measurements by about 25–30%. This discrepancy will be discussed in Section 6.5.

6.5. Variation of steady liquid penetration with ambient density

Fig. 10 shows the computed and measured liquid penetrations as a function of the ambient density. The injection pressure, the ambient temperature and the orifice diameter are 136 MPa, 1000 K and 246 μm, respectively. Based on the atomization model, the size of the injected droplets would decrease proportional to the increase in density. The computed penetrations are shown for the current model that is referred to as the non-equilibrium model, as drop size effects are included, as well as for the equilibrium model [12] where the liquid and the vapor mass fractions were obtained from thermodynamic state relationships. The computed and the measured steady liquid penetrations decrease with increase in the ambient density. Increasing the ambient density increases the mass of the ambient air entrained for the same mass of fuel injected. Therefore, more liquid is vaporized and the liquid penetration decreases. The equilibrium model predicts a smaller rate of decrease in the penetration compared to the measurements. Increasing the density increases the pressure, which increases the saturation temperature and so relatively more mass of liquid is present in the equilibrium mixture [12]. This effect opposes the decrease in the liquid mass due to greater entrainment and vaporization. The fact that the measurements show greater sensitivity of the steady liquid penetration to the ambient density than the equilibrium model suggests that non-equilibrium effects such as the drop size may be important.

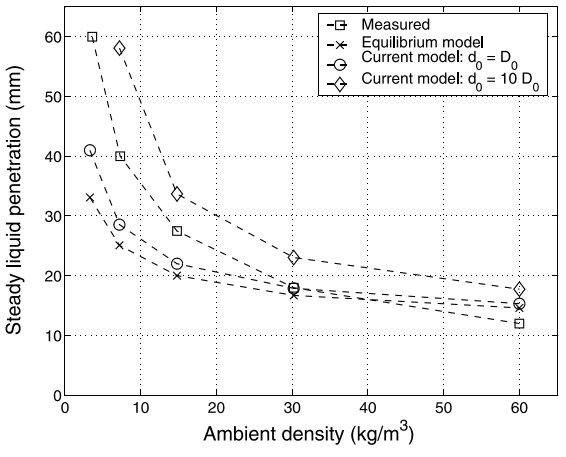

Fig. 10. Steady liquid penetration versus ambient density. $T_a = 1000$ K, $P_{inj} = 136$ MPa, $d_{orif} = 246$ μm.

Fig. 10 shows that the current non-equilibrium model predicts a greater sensitivity of the liquid penetration to the ambient density relative to the equilibrium model, but still the trends are closer to the equilibrium model than the measurements when the injected drop sizes predicted by the atomization model, Eq. (25), are employed. This implies that for the drop sizes predicted by the atomization model under these conditions (0.1–2 μm), vaporization is controlled primarily by entrainment. Therefore, the effect of drop size is not sufficient to predict the measured trends with respect to ambient density. This was the reason for the quantitative discrepancies at lower ambient densities seen in earlier cases. Fig. 10 also shows the computed penetration when the injected drop diameter is increased by a factor of 10 compared to the predicted size, D_0, from the atomization model, Eq. (25). The functional dependence of the injected drop diameter on the ambient density is still preserved, only the constant in Eq. (25) is multiplied by 10. In this case, the computed and the measured variation of the liquid penetrations are almost parallel to each other. The liquid penetrations at the lower densities are greater than what is predicted by the model when smaller drop sizes are injected and the increase in the liquid penetration due to the non-equilibrium drop size effect is greater.

We can also make an observation about the possible injected drop sizes under Diesel conditions. When the injected drop sizes were increased by a factor of 10, the drop sizes ranged from about 1 μm at the highest ambient density of 60 kg/m^3 to about 20 μm at the lowest ambient density of 3.3 kg/m^3. Fig. 10 shows that the drop size range from 1 to 20 μm gives reasonable agreement of trends with the measurements. This is an indirect evidence that the drop sizes after atomization for the range of ambient densities considered here are of the order of 1–20 μm in Sauter mean diameter for the range of conditions considered. Typical Diesel engine conditions are 15–30 kg/m^3 of ambient density and under these conditions the drop sizes would be at most 2–4 μm in Sauter mean diameter . The quantitative values from the measurements and the computations differ by about 40%, with the injected drop diameters of $10D_0$. The current model does not consider the effects of slip velocity between the droplets and the ambient gas. In addition, effects of collisions and coalescence are neglected. These phenomena may increase the liquid penetration further at lower ambient densities with a reduced drop size. So the actual injected drop size range for agreement with the measurements may be even lower than 1–20 μm for ambient densities ranging from 3.3 to 60 kg/m^3 and in that case better quantitative agreement could be expected. The difference in the quantitative values may also be attributed to the uncertainties in the fuel properties and this requires further investigation. We

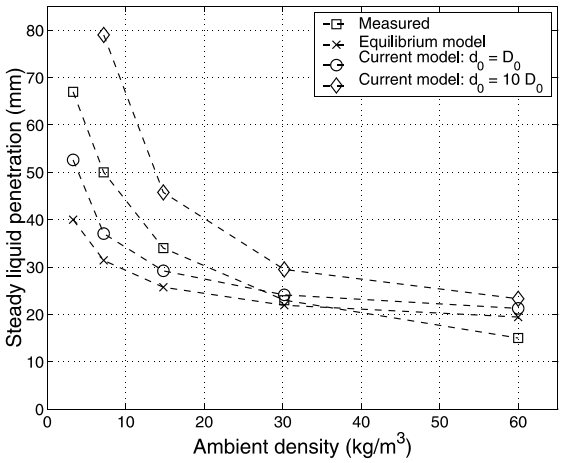

Fig. 11. Steady liquid penetration versus ambient density. $T_a = 850$ K, $P_{inj} = 136$ MPa, $d_{orif} = 246$ μm.

have repeated the computations at a lower ambient temperature of 850 K, keeping the injection pressure and the orifice diameter at 136 MPa and 246 μm, respectively. Fig. 11 shows the computed and measured liquid penetration as a function of the ambient density at an ambient temperature of 850 K. The computed results are presented for the equilibrium model and the non-equilibrium model with injected drop sizes of D_0 and $10D_0$. The trends are similar to the previous case with the higher ambient temperature. The injected drop size range of 1–20 μm shows better agreement of trends with the measurements. In Section 6.6, we discuss the distribution of the mean drop sizes in the chamber for the different ambient densities.

6.6. Comments on the drop size distribution in the chamber under Diesel conditions

In Section 6.5, we drew conclusions regarding the expected injected drop sizes under Diesel conditions. But since the droplets are vaporizing, the mean drop sizes inside the chamber are expected to be lower than the injected drop sizes and may be more characteristic of the behavior of the droplets. We define the Sauter mean diameter, D_{chamb} of the droplets in the chamber as a ratio of the total volume of drops in the chamber to the total surface area of drops in the chamber. More precisely, for spherical droplets, it may be shown that

$$D_{chamb} = \frac{6 \int_V \rho_m Y_l dV}{\rho_l \int_V \rho_m L_s dV} \quad (26)$$

We now look at the variation of D_{chamb} with time for the different ambient density cases. We choose the computations performed with injected drop diameters of $10D_0$, since these gave better agreement in trends of steady liquid penetration with the measurements.

Fig. 12 shows the ratio of $D_{chamber}$ to the injected mean drop diameter, d_0, as a function of time for different ambient densities ranging from 7.2 to 60 kg/m^3. D_{chamb} decreases with time due to vaporization and reaches a steady value that is a fraction of d_0 for all the cases. The steady value is reached in approximately the same time in which the liquid penetration reaches a steady value. The steady value of D_{chamb} depends on the ambient density. The steady value is about 88% of the injected drop diameter for $\rho_a = 60$ kg/m^3 and the fraction decreases with decrease in ambient density. For $\rho_a = 7.2$ kg/m^3, the steady value of D_{chamb} is about 83% of the injected drop diameter. The steady fraction of D_{chamb} to d_0 is a measure of the variance in the drop size distribution in the chamber. At any instant, the largest drop sizes in the chamber are near the injector. So the fraction of D_{chamb} to d_0 is also a measure of the ratio of the mean drop size to the largest drop size in the chamber. This implies that the variance in the drop size distribution is about 12% at the highest ambient density and about 17% at the lowest ambient density considered. Thus, based on these computations, under Diesel conditions, the variance in the chamber drop size distribution is not more than 20% and so most of the drop sizes in the chamber are of the order of the injected drop sizes. This results from rapid vaporization under Diesel conditions because of small drop sizes and high ambient temperatures. Therefore, the only droplets that are present in the chamber are those near the injector that could not vaporize as they could not mix with sufficient hot ambient gases. The variance increases with decreasing ambient density because of the increase in the injected drop sizes. So, the vaporization rates become

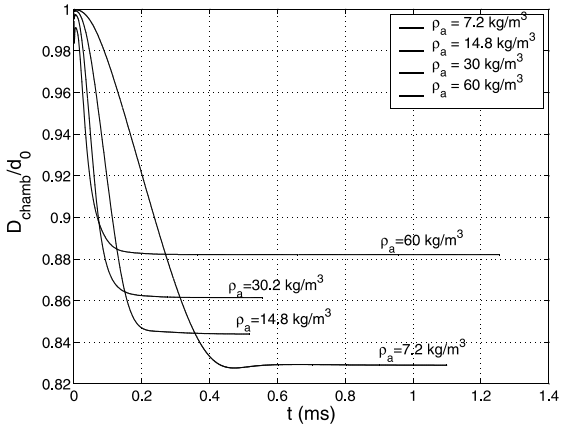

Fig. 12. Ratio of Sauter mean drop diameter in the chamber, D_{chamb}, to injected drop diameter (d_0) for different ambient densities. $T_a = 1000$ K, $P_{inj} = 136$ MPa, $d_{orif} = 246$ μm, $d_0 = 10D_0$.

progressively slower with decrease in ambient density that leads to a wider distribution of drop sizes in the chamber.

7. Summary and conclusions

The liquid-phase penetration in non-combusting vaporizing Diesel sprays is computed using a LHF model. We have evaluated the effects of a non-equilibrium droplet vaporization model on liquid penetration and compared the computed results with laser diagnostics measurements in a constant volume chamber under Diesel conditions. The effects of orifice diameter, injection pressure, ambient temperature and ambient density on the steady liquid penetration are studied and compared with the measurements. The computations show that the steady liquid penetration increases linearly with the orifice diameter, does not vary significantly with injection pressure and decreases with decrease in the ambient temperature. All the above mentioned trends are in agreement with the measured trends. These trends can be explained on the basis of the entrainment characteristics of turbulent jets. The results imply that these LHF computations are able to predict the entrainment characteristics with reasonable accuracy. The effect of drop sizes does not appear to be important in determining the variation of the liquid penetration with orifice diameter, injection pressure and ambient temperature.

The computed liquid penetrations show a lesser sensitivity to ambient density than the measurements when the injected drop sizes originally predicted by the Diesel atomization model are employed but show better agreement when the injected drop sizes are increased by a factor of 10 for all the ambient densities. The change in trend is caused by the fact that the effect of injected drop sizes on the liquid penetration appears to be more important as ambient density is decreased. The study also suggests that the possible range of injected drop sizes in Diesel engines may be between 1 and 4 μm since this range gives reasonable agreement of liquid penetration trends with measurements. An analysis of drop size variation in the chamber shows that the mean drop sizes in the chamber are within 20% of the injected drop sizes for all the ambient density cases considered in this work. Decrease in the ambient density appears to predict a wider distributions of drop sizes.

Acknowledgements

The authors thank the Purdue Research Foundation (PRF), Cummins Engine Company and the Detroit Diesel Corporation for providing financial support for this work.

References

[1] V. Magi, REC-87: a new 3-D code for flows, sprays and combustion in reciprocating and rotary Engines, Mechanical and Aerospace Engineering Report No. 1793, Princeton University, 1987.
[2] V. Magi, REC-2000: a multidimensional code for transient, two-phase turbulent reacting flows, Technical Report, Engine Research Laboratory, School of Mechanical Engineering, Purdue University, 2000.
[3] A. Amsden, KIVA-3: a KIVA program with block-structured mesh for complex geometries, Los Alamos Laboratory Report No. LA-12503-MS, 1993.
[4] P.J. O'Rourke, F.V. Bracco, Modeling of drop interactions in thick sprays and a comparison with experiments, The Institution of Mechanical Engineers, Publication 1980-9, 1980, pp. 101–116.
[5] F.V. Bracco, Modeling of engine sprays, Trans. SAE 94 (1985) 144–167.
[6] R.D. Reitz, Modeling atomization processes in high pressure vaporizing sprays, Atom. Spray Technol. 3 (1987) 309–337.
[7] J. Abraham, What is adequate resolution in the numerical computations of transient jets? Trans. SAE 106 (1997) 141–155.
[8] V. Iyer, J. Abraham, Penetration and dispersion of transient gas jets and sprays, Combust. Sci. Technol. 130 (1997) 315–335.
[9] R. Aneja, J. Abraham, How far does the liquid penetrate in a Diesel engine: computed results vs. measurements? Combust. Sci. Technol. 138 (1998) 233–255.
[10] S. Post, J. Abraham, A computational study of the processes that affect the steady liquid penetration in full-cone Diesel sprays, Combust. Sci. Technol. 165 (2001) 1–40.
[11] D.L. Siebers, Liquid-phase fuel penetration in Diesel sprays, SAE Paper 980809 (1998).
[12] V. Iyer, S. Post, J. Abraham, Is the liquid penetration in Diesel sprays mixing controlled? Proceedings of the Combustion Institute, vol. 28, 2000, pp. 1111–1118.
[13] M. Ishii, Thermo-Fluid Dynamic Theory of Two-Phase Flows, Eyrolles, Paris, 1975.
[14] D.A. Drew, Mathematical modeling of two-phase flow, Ann. Rev. Fluid Mech. 15 (1983) 261–291.
[15] C. Crowe, M. Sommerfeld, Y. Tsuji, Multiphase Flow with Droplets and Particles, CRC Press, Boca Raton, 1998.
[16] M.A. Lopez de Bertodano, Two-fluid model for two-phase turbulent jets, Nucl. Eng. Design 179 (1998) 65–74.
[17] G.M. Faeth, Mixing transport and combustion in sprays, Prog. Energy Combust. Sci. 13 (1987) 293–345.
[18] B.E. Launder, D.B. Spalding, The numerical computation of turbulent flows, Comput. Meth. Appl. Mech. Eng. 3 (1974) 269–289.
[19] S.P. Turns, An Introduction to Combustion: Concepts and Applications, McGraw-Hill, New York, 1996.

[20] J.S. Chin, A.H. Lefebvre, Steady-state evaporation characteristic of hydrocarbon fuel drops, AIAA J. 21 (10) (1983) 1437–1443.
[21] S.V. Patankar, D.B. Spalding, A calculation procedure for heat, mass and momentum transfer in three-dimensional parabolic flows, Int. J. Heat Mass Transfer 15 (1972) 1787–1806.
[22] J. Abraham, Entrainment characteristics of transient gas jets, Numer. Heat Transfer 30 (1996) 347–364.